RESEARCH & DEVELOPMENT IN POWER ENGINEERING, 2019

Development of operation strategy for recompression supercritical CO_2 cycle with intercooled main compressor under off-design condition

Yuegeng Ma[1,2], *Tatiana* Morozyuk[2], *Jiping* Liu[1*]

[1] MOE Key Laboratory of Thermal Fluid Science and Engineering, Xi'an Jiaotong University, Xianning West Road. 28, Xi'an 710049, PR China
[2] Institute for Energy Engineering, Technische Universität Berlin, Marchstr. 18, Berlin 10587, Germany

Abstract. The supercritical carbon dioxide (S-CO_2) cycle is regarded as a potential option for the next generation power conversion system. Concentrated solar power (CSP) plant is one of the promising scenarios to adopt the S-CO_2 cycle due to the appealing thermal efficiency and the ability to integrate thermal storage and dry cooling. Among various cycle configurations of S-CO_2 cycle, the recompression S-CO_2 cycle with intercooled main compressor is one of the optimal choices that can provide superior efficiency and a large enough temperature differential for thermal input, which together contribute to the minimization of the overall levelized cost of electricity (LCOE) of the whole CSP plant. The off-design performance and the associated control scheme have important effects on the CSP plant. This paper develops an off-design model for the recompression S-CO_2 cycle with intercooled main compressor for the commercialized hundred-megawatt CSP plant. The effects of different off-design conditions on cycle performance are first evaluated. Different operating strategies regarding the control of cycle maximal pressure and preventing abnormal compressor conditions during off-design operation are then presented and compared. This work is expected to provide knowledge for the optimal control of recompression S-CO_2 cycle with intercooled main compressor during the real operation of the CSP plant.

1. Introduction

Concentrated solar power (CSP) is deemed as a promising renewable energy technology that is likely to play the role of middle-load or even base-load power source in the future energy mix [1]. The CSP plant utilizes heating media such as molten salts to transfer solar energy to the power block. Depending on the upper-temperature limits of the adopted heating media, the power block could be operated at various maximal temperature levels ranging from 350 to over 700 °C [2]. In this temperature range, the S-CO_2 cycle has been regarded as a superior option for the power block in the CSP plant due to its better efficiency and simpler configuration among various choices [3,4].

While many published works focusing on the parametric analyses and optimization of the S-CO_2 cycle, further studies on the off-design characteristics and developments of cycle control strategies were not gained enough attention. The S-CO_2 cycle in the CSP plant is usually operated under off-design conditions due to the changes of ambient conditions in the cold end of the cycle and the inlet temperature and mass flowrate of heating media in the cycle hot end. Therefore, the investigation of the off-design performance and development of the associated control strategies are expected to contribute to the improvement of the actual performance during operation. According to the authors' knowledge, the previous off-design performance studies were only done for the recompression S-CO_2 cycle and simple-recuperated cycle with limited consideration on the effects of various control strategies on the cycle performance [5–7]. Many previous studies suggested that the recompression with intercooled main compressor (ICMC) was the most promising cycle configuration due to the superior performance and large temperature differential for the integration of the thermal storage system [8,9].

In this work, an off-design model is proposed for the recompression cycle with ICMC. The operational issues of the main compressor (MC) are highlighted in the off-design model. four control strategies and the associated configurations are proposed and compared to determine the optimal off-design operating solution with superior efficiency and no risks of damaging MC.

2. System description

The schematic of the S-CO_2 recompression cycle with ICMC and its corresponding T-S diagram are presented in Fig.1. The design parameters of the S-CO_2 recompression cycle with ICMC are listed in Table 1. The elaborative introduction of the thermodynamic characteristics of this cycle is presented in our previous work [9]. Compared to the classic recompression cycle, the introduction of ICMC lead to both higher energetic efficiency and larger temperature differential across the primary heat exchanger (PHX), which contributes to lower LCOE of the whole CSP plant [9]. Split shaft configuration is used for the cycle system due to the

benefits in terms of efficiency and control perspectives for such large-scale plants [10]. A synchronous generator is configured for this turbine and variable-speed drive motors are used for the recompressor and main compressor. A buffer tank is configured upstream of the MC to stabilize the compressor inlet pressure at the specified value by inventory control [11].

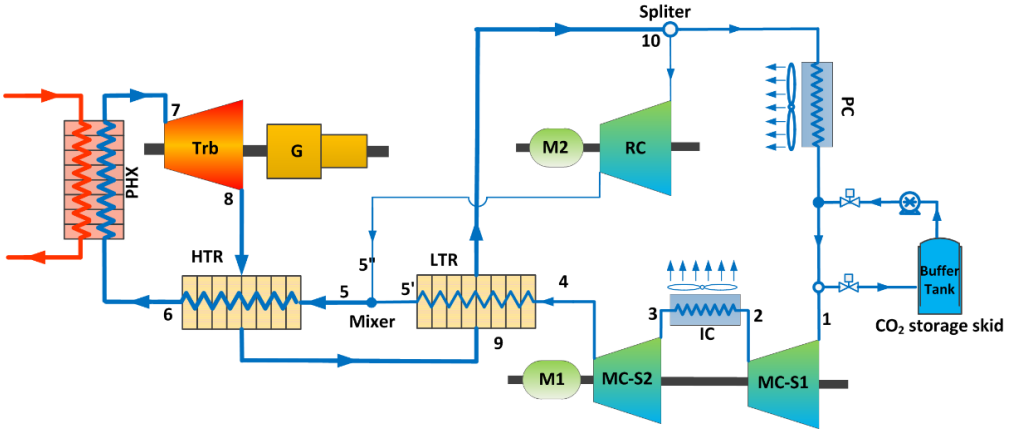

Fig. 1 Configuration of recompression cycle with ICMC

Table 1 Input parameters for the design parameters of the S-CO_2 recompression cycle with ICMC [9]

Input Parameter\ Symbol	Unit	Value
Net output power	MW	100
Temperature of hot storage tank	°C	565
Turbine inlet temperature	°C	550
Main Compressor outlet pressure	MPa	25
Cooler cold-end temperature approach	°C	15
Turbine isentropic efficiency	%	93
Compressor isentropic efficiency	%	89
Pressure drop in PHX	kPa	50
Hot-side Pressure drop of HTR	kPa	60
Cold-side Pressure drop of HTR	kPa	30
Hot-side pressure drop of LTR	kPa	20
Cold-side pressure drop of LTR	kPa	40
Pressure drop in the cooler	kPa	20
Pinch-point temperature approach	°C	5

3. Model implementation

The model of each component and the implementation of cycle simulation under design condition has been detailed in the previous work [9]. This section presented the off-design model of each crucial components in the cycle and the implementation of cycle off-design simulation. These off-design models for components are established in MATLAB 2018a using an objected-oriented approach. REFPROP is used to obtain the necessary thermal properties of CO_2 [12].

3.1 Component model

▪ *Turbine*

Due to the hundred-megawatt level output power, the multi-axial flow turbine is chosen for the cycle in views of higher efficiency and relatively steady flow [13]. Stodola's ellipse method is applied to obtain the turbine inlet pressure under off-design conditions [14,15]. The turbine is assumed to work under the sliding mode with a fixed nozzle area [14]. According to Stodola's ellipse method, the relationship between the mass flow coefficient under design (ϕ_d) and off-design (ϕ_{od}) conditions can be described as follow.

$$\frac{\phi_{od}}{\phi_d}=\frac{\sqrt{1-\left(\frac{p_{out,od}}{p_{in,od}}\right)^2}}{\sqrt{1-\left(\frac{p_{out,d}}{p_{in,d}}\right)^2}} \tag{1}$$

where ϕ is defined as

$$\phi=\dot{m}_{in}\cdot\frac{\sqrt{T_{in}}}{p_{in}} \tag{2}$$

Substituting the above two equations, $p_{in,od}$ can be obtained as

$$p_{in,od}=\sqrt{m_{in,od}^2\cdot T_{in,od}\cdot Y_d+p_{out,od}^2}\ \text{ with } Y_d=\frac{p_{in,d}^2-p_{out,d}^2}{p_{in,d}^2\cdot\phi_d^2} \tag{3}$$

The turbine isentropic efficiency under off-design conditions ($\eta_{T,od}$) can be obtained as follows.

$$\eta_{T,od}=\eta_{T,d}\cdot\sin\left[0.5\pi\left(\frac{\dot{m}_{in,od}\cdot\rho_{in,od}}{\dot{m}_{in,d}\cdot\rho_{in,d}}\right)^{0.1}\right] \tag{4}$$

where $\rho_{in,od}$ and $\rho_{in,d}$ are the density of CO_2 under design and off-design conditions.

▪ *Compressor*

The off-design model of compressor adopted here is based on the nondimensionalized empirical equation regressed out of the experimental data from SNL compressor developed by Dyreby [5]. The flow coefficient of the compressor is defined as

$$\phi_C=\frac{\dot{m}}{\rho_{in}U_{in}D_{in}^2} \tag{5}$$

where U_{in} is the inlet velocity and D the inlet diameter of the compressor.

$$U_{in} = \frac{D_{in}}{2} N \tag{6}$$

The ideal head coefficient (ψ_C) is defined as

$$\psi_C = \frac{(h_{out} - h_{in})}{U_{in}^2} \tag{7}$$

where h_{in} and h_{out} are the enthalpies of CO_2 at the inlet and outlet of the compressor.

To consider the effect of shaft speed (N) on the off-design performance, ϕ_C, ψ_C and the compressor isentropic efficiency (η_C) are modified as Eqs. (8) through (10), and the performance of compressor can be mapped with polynomial regression as Eqs. (11) and (12)

$$\phi_C^* = \frac{\dot{m}}{\rho_{in} U_{in} D_{in}^2} \left(\frac{N}{N_d} \right)^{1/5} \in [0.02, 0.05] \tag{8}$$

$$\psi_C^* = \frac{(h_{out} - h_{in})}{U_{in}^2} \left(\frac{N_d}{N} \right)^{\left(20\phi_C^*\right)^3} \tag{9}$$

$$\eta_C^* = \eta_C \left(\frac{\eta_{C,D,0}}{\eta_{C,D}} \right) \left(\frac{N_d}{N} \right)^{\left(20\phi^*\right)^5} \tag{10}$$

$$\eta_C^* = -0.7069 + 168.6\phi_C^* - 8089\phi_C^{*2} + 182725\phi_C^{*3} - 1638000\phi_C^{*4} \tag{11}$$

$$\psi_C^* = -0.04049 + 54.6\phi_C^* - 2505\phi_C^{*2} + 53224\phi_C^{*3} - 498626\phi_C^{*4} \tag{12}$$

▪ *Heat Exchanger*

The model of heat exchanger here is applied to the high-temperature recuperator (HTR), low-temperature recuperator (LTR) and the primary heat exchanger (PHX). The heat sink is assumed to keep constant cold-end temperature difference through the adjustment of the mass flow rate of cooling air through the cooler. The off-design model of heat exchanger consists of two parts, i.e., the pressure sub-model for the pressure loss (Δp) and heat transfer sub-model for the conductance of heat transfer (UA). Depending on the thermodynamic states of CO_2 through the heat exchanger, the model considers the effects of thermal property variation on the Δp and UA differently. The CO_2 thermal properties through the HTR and PHX change uneventfully because the operating condition is far away from the critical region. The conductance of heat transfer (UA_{od}) and pressure loss (Δp_{od}) under off-design conditions is therefore calculated without considering the effects of thermal properties variation as follows.

$$\frac{UA_{od}}{UA_d} = \frac{\dot{m}_{c,d}^{-0.8} + \dot{m}_{h,d}^{-0.8}}{\dot{m}_{c,od}^{-0.8} + \dot{m}_{h,od}^{-0.8}} \tag{13}$$

$$\frac{\Delta p_{od}}{\Delta p_d} = \left(\frac{\dot{m}_d}{\dot{m}_{od}} \right)^{7/4} \tag{14}$$

Unlike the cases for the HTR and PHX, the CO_2 through the LTR is close to its critical point. The thermal properties relating to heat transfer and hydraulic characteristic undergo drastic changes with temperature and pressure should be considered in the UA calculation under off-design conditions. Therefore, the UA_{od} and Δp_{od} are calculated as follows [7].

$$\frac{UA_{od}}{UA_d} = \frac{\alpha_{c,d}^{-1} + \alpha_{h,d}^{-1}}{\alpha_{c,od}^{-1} + \alpha_{h,od}^{-1}} \text{ with } \alpha = \dot{m}^{0.8} c_p^n k^{(1-n)} \mu^{(n-0.8)} \tag{15}$$

$$\frac{\Delta p_{od}}{\Delta p_d} = \left(\frac{\dot{m}_d}{\dot{m}_{od}} \right)^{7/4} \cdot \left(\frac{\mu_d}{\mu_{od}} \right)^{1/4} \cdot \left(\frac{\rho_d}{\rho_{od}} \right)^{-1} \tag{16}$$

where c_p is the specific heat capacity, k is the coefficient of heat conductivity. μ is the dynamic coefficient of viscosity. n=0.4 for heating fluid and n=0.3 for cooling fluid.

4. Results and discussion

The cycle performance under various off-design conditions is investigated in this section. Parametric optimizations are first implemented for three cases with different MC inlet temperature ($T_{MC,in,d}$) to obtain optimal design points. The effects of $T_{salt,in}$, $\dot{m}_{salt}$ and $T_{MC,in}$ on the off-design performance are then studied with sensitivity analysis in their respective ranges as presented in Table. 2. In the following off-design calculation under different conditions, only the results without abnormal conditions of the MC are presented in the figures.

Table 2 Variation ranges of parameters for off-design study

Parameter	Unit	Design point	Off-design range
$T_{salt,in}$	°C	565	535-595
Relative m_{salt}	\	1	0.6–1.2
$T_{MC,in}$	°C	32,41,50	32–50

4.1 Off-design performance under varying heat source conditions

Fig. 2–3 presents the off-design performance with the change of $T_{salt,in}$ under the three conditions of $T_{MC,in,d}$. It is found that the cycle can be operated normally in the whole range of $T_{salt,in}$ with these four control schemes under three conditions of $T_{MC,in,d}$. The η_{cyc} and $\dot{W}_{net}$ increase linearly with the rise of $T_{salt,in}$ for all the cases. The variation of the studied variables show similar variation tendencies with $T_{salt,in}$ for the three $T_{MC,in,d}$ cases with slight differences observed among different control schemes. As illustrated in Fig. 2, the variation of p_{max} in the range of $T_{salt,in}$= 535 °C–595 °C is less than 0.3MPa for the cases of the FP control scheme and the change of relative shaft speed (RN) is less than 0.3%. The comparisons between B_FP and M_FP and between B_SP and M_SP show that the configuration of MC, i.e., basic configuration or modified configuration have no effects in control strategy and hence no effects on the

cycle performance because only the control of N is implemented for both basic and modified configurations during off-design condition of $T_{\mathrm{salt,in}}$. The comparisons between B_FP and B_SP and between M_FP and M_SP indicate that the $\dot{W}_{\mathrm{net}}$ with different pressure control schemes have slight difference in the rate of change with $T_{\mathrm{salt,in}}$. As shown in Fig.3, the $\dot{W}_{\mathrm{net}}$ increases at higher rate under SP control than under FP control. This can be attributed to the higher decreasing rate of $\dot{m}_{\mathrm{CO2}}$ with FP control which partially counteracts the effects of η_{cyc} on $\dot{W}_{\mathrm{net}}$.

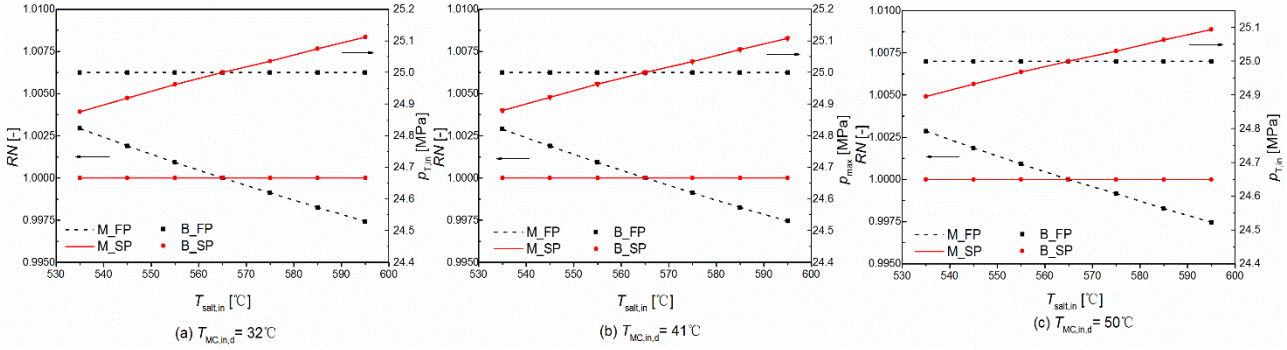

Fig. 2 The variations of RN and $p_{\mathrm{T,in}}$ with $T_{\mathrm{salt,in}}$

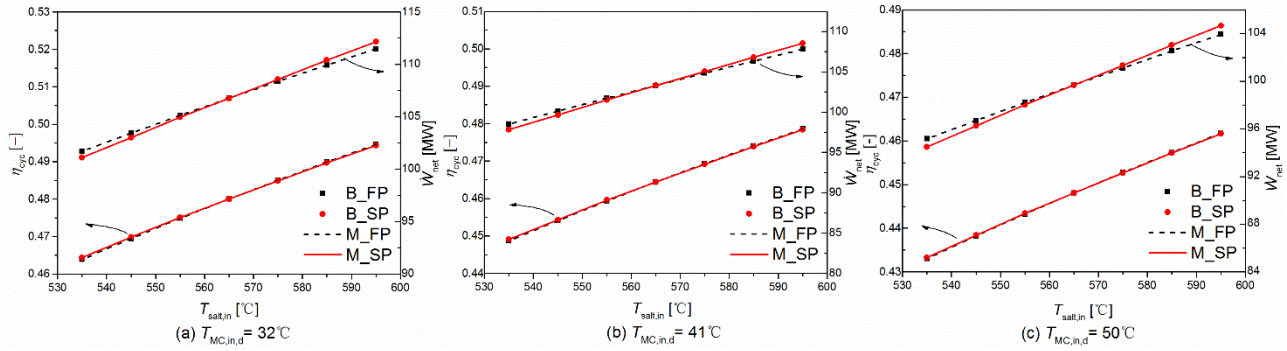

Fig. 3 The variations of $\dot{W}_{\mathrm{net}}$ and η_{cyc} with $T_{\mathrm{salt,in}}$

Fig. 4–5 presents the effect of $\dot{m}_{\mathrm{salt}}$ on the off-design performance of cycle. The cycle can be operated in the whole range of $T_{\mathrm{salt,in}}$ with these four control schemes and three $T_{\mathrm{MC,in,d}}$ conditions. As shown in Fig. 4, The η_{cyc} and $\dot{W}_{\mathrm{net}}$ increase monotonously with $\dot{m}_{\mathrm{salt}}$ at a decreasing rate. The comparisons between B_FP and M_FP and between B_SP and M_FP indicate that the configurations have no effect on the off-design performance as only the N is used as control variable during off-design operation. The comparisons between B_FP and B_SP and between M_FP and M_FP indicate that the FP control leads to lower η_{cyc} yet higher $\dot{m}_{\mathrm{CO2}}$ than SP control when $\dot{m}_{\mathrm{salt}}$ decreases, and these differences are more significant as $\dot{m}_{\mathrm{salt}}$ reduces. As the decreased η_{cyc} offsets the effect of increased $\dot{m}_{\mathrm{salt}}$, the $\dot{W}_{\mathrm{net}}$ of FP control is only slightly higher than that of SP control when $\dot{m}_{\mathrm{salt}}$ is lower than the design value and the difference in $\dot{W}_{\mathrm{net}}$ become less significant as $\dot{m}_{\mathrm{salt}}$ rise. (see Fig. 5)

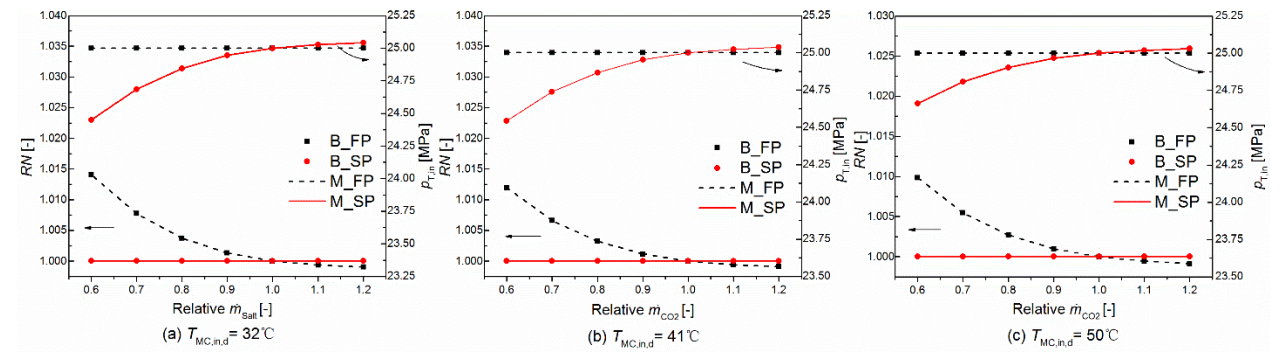

Fig. 4 The variations of RN and $p_{\mathrm{T,in}}$ with $\dot{m}_{\mathrm{salt}}$

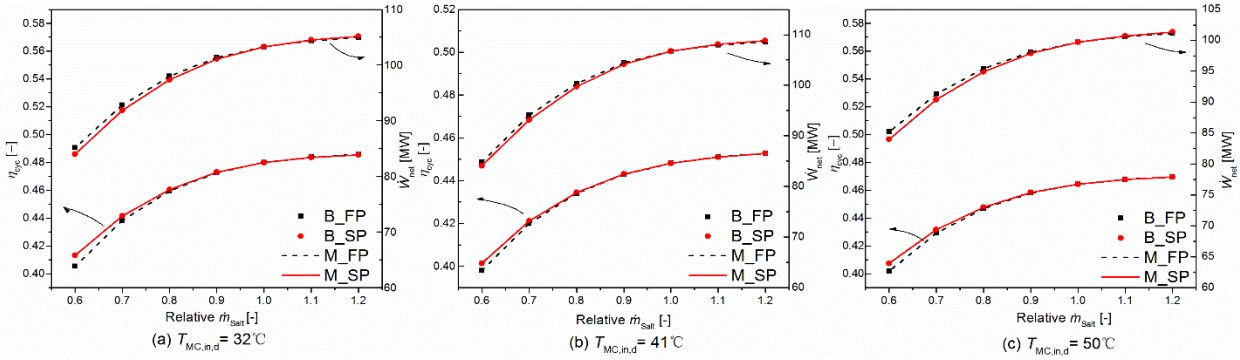

Fig. 5 The variations of $\dot{W}_{net}$ and η_{cyc} with $\dot{m}_{salt}$

4.2 Off-design performance under varying ambient conditions

Fig. 6–7 presents the cycle off-design performance under different MC inlet temperature conditions. Unlike the relative uneventful effects of $\dot{m}_{salt}$ and $T_{salt,in}$, the impact of $T_{MC,in}$ variations on cycle performance is significant. The change of $T_{MC,in}$ results in variations of cycle performance with different fashions from one another for these cases with different control schemes and $T_{MC,in,d}$. The comparisons between B_FP and M_FP and between B_SP and M_SP show that the basic configurations cannot be applied under low $T_{MC,in}$ off-design conditions for the cases of $T_{MC,in,d}$=41 °C and 50 °C, with a larger applicable range for B_FP than B_SP; on the contrary, the modified configurations can cover all the studied range in three cases with recirculation system of MC being activated to prevent surge for low $T_{MC,in}$ off-design conditions when $T_{MC,in,d}$=41 and 50 °C. According to the comparisons of B_FP versus B_SP and M_FP versus M_SP, it is found that the pressure control strategy has a significant effect under the off-design conditions of $T_{MC,in}$. The FP control generally results in better η_{cyc} than that of FP control especially when the $T_{MC,in}$ is significantly deviated from the $T_{MC,in,d}$. Under off-design conditions of $T_{MC,in}$, the $\dot{W}_{net}$ under SP control deviates apparently from the design point value whereas the $\dot{W}_{net}$ under FP control undergoes relatively mild change. This is partially due to the different trends of $\dot{m}_{CO2}$ variation during off-design operation besides the effect of η_{cyc}. The $\dot{m}_{CO2}$ is controlled at almost constant value under FP control. By comparison, the $\dot{m}_{CO2}$ under SP control varies significantly as $T_{MC,in}$ changes under off-design conditions due to the varying $p_{T,in}$ under off-design conditions. The use of SP control also lead to more significant variations in $T_{T,in}$ and $T_{salt,out}$, which may cause adverse effects on the performance of solar components.

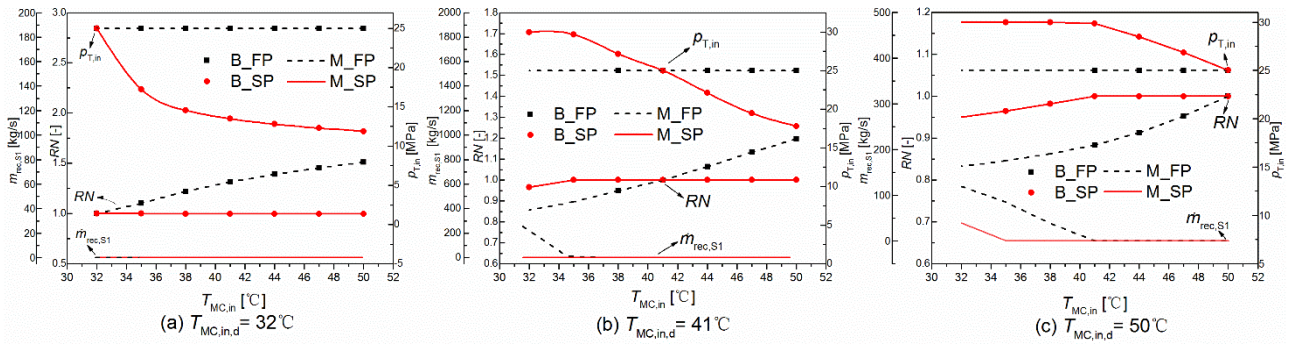

Fig. 6 The variations of RN and $p_{T,in}$ with $T_{MC,in}$

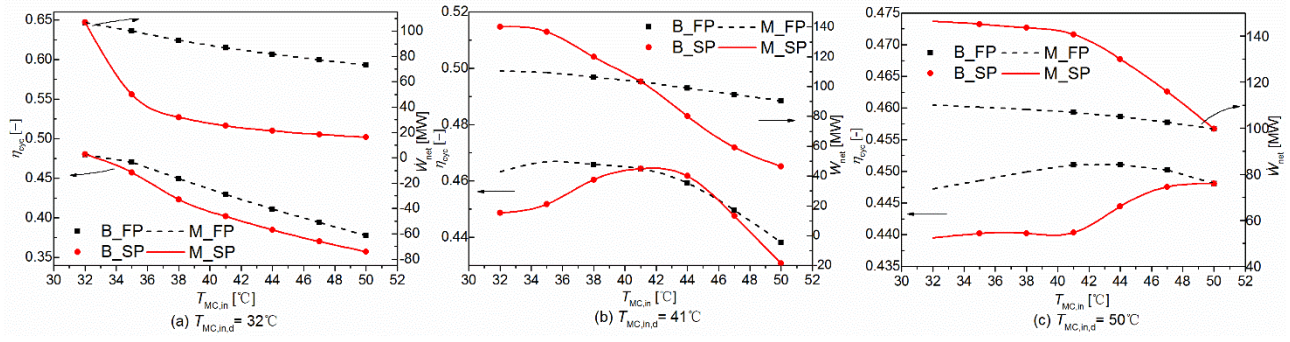

Fig. 7 The variations of $\dot{W}_{net}$ and η_{cyc} with $T_{MC,in}$

5. Conclusion

This study establishes an off-design model for the S-CO_2 cycle with ICMC. The potential issues of the MC abnormal operation were highlighted, four control schemes and the associated configurations for MC are developed and compared. The off-design performance under conditions of varying $T_{salt,in}$, $\dot{m}_{salt}$ and $T_{MC,in}$ are investigated for three cases with different $T_{MC,in,d}$. The following conclusions are drawn after this study:

- The changes of $T_{salt,in}$ and $\dot{m}_{salt}$ under off-design conditions in the cycle hot end lead to uneventful effects in terms of the MC control. No abnormal operation conditions are observed for MC. The MC configuration cycle performance has no effect on cycle performance, while the pressure control strategy has very slight effects.
- The change of $T_{MC,in}$ under off-design conditions significantly affects the MC control. The S-CO_2 cycle with a high $T_{MC,in,d}$ will run into the abnormal condition of MC surge under low $T_{MC,in}$ conditions when integrated with basic configuration of MC. In contrast, the cycle with modified MC configuration can prevent the surge risk by recirculating partial working fluids.
- During all these off-design analyses on $T_{salt,in}$, $\dot{m}_{salt}$ and $T_{MC,in}$, only single mode is required for MC. The parallel compressor is not activated for either S1 or S2 of the modified configuration. The risk of zero pressure head under the conditions of $T_{MC,in} > T_{MC,in,d}$ can be prevented by N control without the use of parallel compressor, and the N can be over 1.5 times of the N_d.
- The off-design analyses show that the M_FP as the control scheme can results in superior efficiency, steady $\dot{W}_{net}$ and no risk of abnormal MC condition under off-design conditions than the other three schemes. However, the cycle performance may be further improved when the real-time parametric optimization is applied for the cycle during off-design conditions.

References

[1] Mehos M, Turchi C, Vidal J, Wagner M, Ma Z, Ho C, et al. Concentrating Solar Power Gen3 Demonstration Roadmap. *NREL Tech Rep*, pp.1–140, (2017).

[2] Philibert, C. Technology roadmap: concentrating solar power. *OECD/IEA*, (2010).

[3] Turchi CS, Ma Z, Neises T, Wagner M. Thermodynamic Study of Advanced Supercritical Carbon Dioxide Power Cycles for High Performance Concentrating Solar Power Systems. *Proc. ASME 2012 6th Int. Conf. Energy Sustain.*, San Diego, CA, USA, (2012).

[4] Crespi F, Gavagnin G, Sánchez D, Martínez GS. Supercritical carbon dioxide cycles for power generation: A review. *Appl Energy*, Vol. 195, pp.152–83. (2017);

[5] Dyreby JJ. Modeling the Supercritical Carbon Dioxide Brayton Cycle with Recompression. *The University of Wisconsin-Madison*, (2014).

[6] Wright SA, Davidson CS, Husa C. Off-design performance modeling results for a supercritical CO_2 waste heat recovery power system. *6th Int. Supercrit. CO_2 Power Cycles Symp.*, pp.1–10. Pennsylvania, USA (2018)

[7] de la Calle A, Bayon A, Soo Too YC. Impact of ambient temperature on supercritical CO_2 recompression Brayton cycle in arid locations: Finding the optimal design conditions. *Energy*, Vol.153, pp.1016–27. (2018)

[8] Wang, Kun, Ming-Jia Li, Jia-Qi Guo, Peiwen Li, and Zhan-Bin Liu. A systematic comparison of different S-CO2 Brayton cycle layouts based on multi-objective optimization for applications in solar power tower plants. *Appl Energy*, Vol.212, pp.109–21, (2018).

[9] Ma Y, Morozyuk T, Liu M, Yan J, Liu J. Optimal integration of recompression supercritical CO_2 Brayton cycle with main compression intercooling in solar power tower system based on exergoeconomic approach. *Appl Energy*, Vol.242, pp.1134–54, (2019)

[10] Weiland N, Thimsen D. A Practical Look at Assumptions and Constraints for Steady State Modeling of sCO_2 Brayton Power Cycles. *No. NETL-PUB-20271. NETL,* (2016).

[11] Held, Timothy J. Initial test results of a megawatt-class supercritical CO_2 heat engine. *4th International Symposium on Supercritical CO_2 Power Cycles*, (2014).

[12] Lemmon EW, Huber ML, Mclinden MO. NIST Reference Fluid Thermodynamic and Transport Properties. *REFPROP database* 23: v7, (2002)

[13] Sienicki JJ, Moisseytsev A, Fuller RL, Wright SA, Pickard PS. Scale Dependencies of Supercritical Carbon Dioxide Brayton Cycle Technologies and the Optimal Size for a Next-Step Supercritical CO_2 Cycle Demonstration. *3th International Symposium on Supercritical CO_2 Power Cycles*, (2011).

[14] Li H, Yang Y, Cheng Z, Sang Y, Dai Y. Study on off-design performance of transcritical CO_2 power cycle for the utilization of geothermal energy. *Geothermics*, Vol. 71, pp.369–79, (2018);

[15] D. COOLKE. Modeling of off-design multistage turbine pressures by Stodola's ellipse. *Energy Incorporated PEPSE User's Group Meeting*. Richmond, VA, Nov, pp. 2-3. (1983).